AAPS PharmSciTech (2022) 23: 141
https://doi.org/10.1208/s12249-022-02261-5

RESEARCH ARTICLE

Theme: Advancements in Amorphous Solid Dispersions to Improve Bioavailability

Stiripentol Enteric Solid Dispersion-Loaded Effervescent Tablets: Enhanced Dissolution, Stability, and Absorption

Ying Wang[1] · Siyuan Xu[1] · Ziyue Xiao[1] · Yuxin Jiang[1] · Qi Jiang[1] · Jun Li[2] · Wei He[1]

Received: 8 January 2022 / Accepted: 20 March 2022 / Published online: 10 May 2022

Abstract

Due to poor solubility and stability in acid conditions, the gastrointestinal administration of stiripentol (STP) is still a significant challenge. This study aimed to explore the applicability of effervescent tablets compressed from STP-loaded enteric solid dispersions to improve the solubility and stability of the insoluble and acid-labile drug. STP-loaded solid dispersions (STP-SDs) and the effervescent tablets (STP-SD-ETs) were prepared using solvent evaporation and dry granulation technology, respectively, and their formulations were optimized. Then, STP-SDs were characterized regarding solid state, *in vitro* release, stability, etc. Results showed that enteric amorphous STP-SDs were successfully prepared and significantly improved the solubility and stability of STP. Moreover, compared with STP suspensions, the bioavailability of STP-SD-ETs was as high as 138.71%. Concomitantly, STP-SD-ETs significantly increased the intestinal absorption rate of STP. Overall, the oral preparation encompassing enteric solid dispersion combined with effervescent tablet technology possesses excellent performance in enhancing dissolution, anti-acid hydrolysis stability, and absorption of STP. Our work provides a promising method to improve the delivery of drugs with poor solubility and acid-labile stability.

KEY WORDS stiripentol · solid dispersions · amorphous · effervescent tablets · epilepsy

INTRODUCTION

Dravet syndrome (DS) is a progressive and epileptic encephalopathy that begins in infancy (1), which is usually accompanied by severe intellectual and motor disability and a high fatality rate (15%) caused by status epilepticus or sudden accidental death from epilepsy (2–5). Stiripentol (STP) is specifically used as an adjuvant DS therapy, which exerts anti-epileptic effects by enhancing the GABAergic neurotransmitters to inhibit the abnormal electrical activity of the brain (6–8). Despite the emergence of two strong competitors (cannabidiol and fenfluramine) in recent years, the efficacy of cannabidiol seems to be modest, while fenfluramine is occasionally ineffective (2, 9). In addition, only STP is suitable for infants under 2 years old and/or with severe status epilepticus (2).

STP is a compound with low water solubility (0.405 mg/mL) and high permeability (log $P = 3.01$), of which the slow and incomplete dissolution in the intestinal milieu is the rate-limiting step for its absorption (10). Moreover, due to the aromatic allyl alcohol structure, STP is prone to chemically reacting with gastric acid, thus causing its poor efficacy (7, 8). The above two shortcomings lead to low oral bioavailability (20%) (8). Therefore, commercial preparations of STP, Diacomit®, generally require high doses (up to 3 g/day) (3) and must be taken with meals (to prevent being destroyed by gastric acid), resulting in troublesome dose-related adverse reactions and poor patient compliance (2, 3, 5, 8, 11). Nonetheless, many attempts have been adopted to enhance drug solubility and gastric instability (12, 13), mainly by using polymeric micelles (14), nanoemulsions (15), protein-stabilized drug particles (16), liposomes (17),

Theme: Advancements in Amorphous Solid Dispersions to Improve Bioavailability

✉ Jun Li
lijunnu@163.com

✉ Wei He
weihe@cpu.edu.cn

[1] Department of Pharmaceutics, School of Pharmacy, China Pharmaceutical University, Nanjing 211198, China

[2] Children's Hospital of Nanjing Medical University, Nanjing, China

etc. However, these systems have limitations such as complex synthesis steps of materials used (14), poor material safety (18), reduced drug permeability (19), low drug loading (20), and easy dissociation or aggregation in physiological solutions (19, 20). Hence, it is necessary to develop new delivery strategies to improve solubility and gastric instability, which may benefit from improving its bioavailability.

Solid dispersion (SD) refers to a solid system in which the active ingredients are uniformly dispersed in a carrier with a highly dispersed state (21). SD technique has been broadly used to enhance dissolution and bioavailability of poorly soluble drugs (22–26), delay drug release (27–29), and increase drug stability (30–32). Synchronously, the SD is expected to promote drug absorption by dissolving the medicament and the polymer matrix to form a supersaturated solution and maintaining this supersaturation state (33). The production of a supersaturated drug solution can increase the absorption rate in the gastrointestinal tract (34). So far, more than twenty SD products have been marketed (35). As an intermediate of pharmaceutical preparations, SD usually needs to be made into tablets or capsules for oral administration. Among them, children broadly accept effervescent tablets due to their excellent taste, convenient taking, greater stability, faster drug absorption, and suitability for people who cannot swallow solid preparations (36–38).

Therefore, an innovative oral formulation of STP based on enteric solid dispersion and effervescent tablets (STP-SD-ETs) was developed in this work. In this study, the formulation of enteric STP solid dispersions (STP-SDs) was first screened. Afterward, the STP-SDs regarding the properties, including surface morphology, amorphous state, resistance to acid hydrolysis, storage stability, and dissolution behavior, were characterized. Finally, we assessed the pharmacokinetics and intestinal absorption mechanism of the optimized formulation (Fig. 1).

MATERIALS AND METHODS

Materials

STP and xanthone (internal standard) were obtained from Macklin Biochemical Co., Ltd. (Shanghai, People's Republic of China). Eudragit L100 was purchased from Shin-Etsu Co. (Tokyo, Japan). Lactose monohydrate, Mannitol, and Povidone K30 were purchased from Chineway Pharmaceutical Technology Co., Ltd. (Shanghai, People's Republic of China). Sodium carboxymethylcellulose (CMC-Na) was from Anhui Sunhere Pharmaceutical Excipients Co., Ltd. (Anhui, People's Republic of China). Anhydrous citric acid and sodium bicarbonate were purchased from Nanjing Reagent Co., Ltd. (Nanjing, People's Republic of China). Deionized water was prepared by a Milli-Q water purifier (EMD Millipore, Billerica, MA, USA). High-performance liquid chromatography (HPLC)-grade methanol was obtained from TEDIA (America, Ohio). All other chemicals were of analytical grade and used as received.

Nanjing Qinglongshan Animal Breeding Institute provided male Sprague–Dawley rats (210 ± 20 g). Animals were kept under controlled environmental conditions (ambient temperature, 24–25 °C; humidity, 50–60%; 12/12-h light/dark cycle) and had free access to standard laboratory food and clean tap water. This study was approved by the Experimental Animal Ethics Committee of China Pharmaceutical University.

Preparation and Formulation Screening of STP-SDs

STP-SDs were prepared using the solvent evaporation method. Briefly, STP and Eudragit L100 were added in an appropriate amount of mixed solvent (ethanol:dichloromethane = 1:1, v/v) in sequence and dissolved completely by ultrasound. The organic solvent was

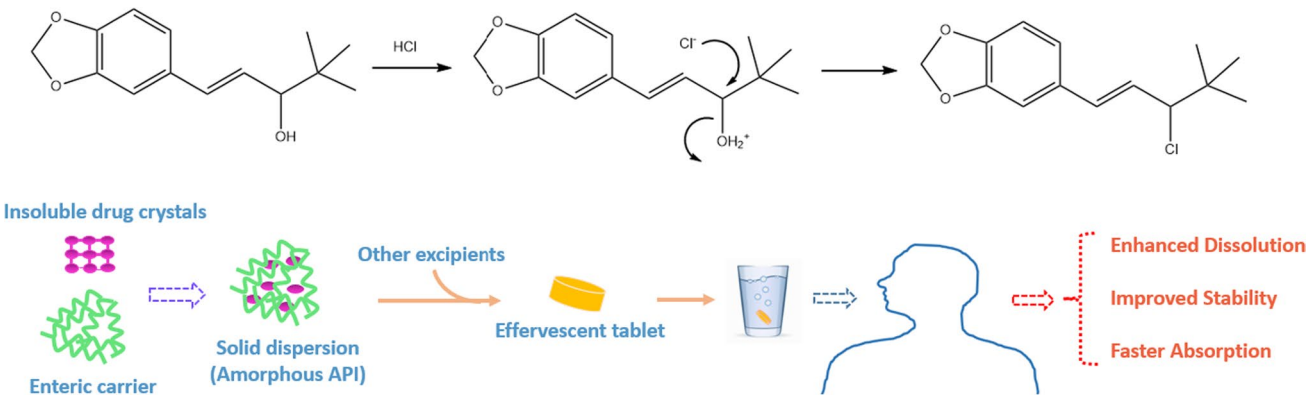

Fig. 1 Schematic illustration of STP-SD-ETs preparation: the acidolysis route of STP and approach for bioavailability enhancement via enteric SDs and effervescent technology. STP-SD-ETs, effervescent tablets containing enteric stiripentol-loaded solid dispersions

removed under vacuum at a temperature of 45 °C and a rotation speed of 180 rpm on a rotary evaporator. The resulting dried solid system was stored in a desiccator at room temperature for 24 h before being crushed and sieved through 80-mesh. For the preparation of the physical mixture (PM), the drug and the carrier sieved through 80-mesh were geometrically mixed in a mortar for 10 min. The prepared SD and PM were stored in a desiccator for subsequent use. STP and Eudragit L100 were prepared as solid dispersions in mass ratios of 1:1, 1:2, 1:3, 1:4, and 1:5, respectively. Then, the saturation solubility and dissolution tests were performed to optimize the formulation.

Solid State Characterization of STP-SDs

Scanning Electron Microscopy (SEM)

The surface morphology of STP and STP-SDs was probed on a scanning electron microscope (Hitachi S-4800). Before the microscopic inspection, the dried sample was dipped into conductive glue and sputtered coating with gold. The micrographs were taken at excitation voltages of 3.0 kV and 5.0 kV, and the magnifications chosen were 2000× and 100×.

X-Ray Powder Diffraction (XRD)

The Bruker D8 Advance X-ray diffractometer was used to characterize the X-ray patterns of STP, Eudragit L100, PM, and STP-SDs to confirm the amorphization of the drug and its molecular dispersion in the polymer matrix. The sample was firstly packed into a 0.5-mm-deep graphite sample holder and then scanned in the 2θ range of 3–50° at a scanning speed of 1°/min, with a step size of 0.02° and a step time of 1 s. The patterns were collected with monochromatic Cu-Kα radiation ($\lambda = 0.154$ nm) at 40 kV and 60 mA.

Differential Scanning Calorimetry (DSC)

The powdered STP, Eudragit L100, PM, and STP-SDs (3–5 mg) were sealed in an aluminum pan and heated at a constant rate of 10 °C/min in the temperature range of 30–300 °C. NETZSCH DSC 204 differential thermal analyzer was used to obtain their thermograms. The thermal analysis data was recorded using the TA 50I PC system with the Shimadzu software program. Indium standards were employed to calibrate DSC temperature and enthalpy standards, and N_2 was used as the purge gas at a 50 mL/min rate.

Fourier-Transform Infrared (FTIR)

In order to study whether there is an interaction between the drug and the carrier, powdered STP, Eudragit L100, PM, and STP-SDs were respectively mixed with potassium bromide (KBr) and compressed into disks. Each sample was scanned 20 times on average with a scan range of 4000–450 cm^{-1} and a resolution of 1.0 cm^{-1}. Bruker TENSOR 27 infrared spectrometer was used to detect its infrared spectrum.

Quantification of STP

In Vitro Sample Quantification

The concentration of STP-SD formulations and other *in vitro* samples was determined by ultraviolet–visible (UV) spectrophotometry. 0.33 mL, 1.67 mL, 3.33 mL, 5.00 mL, 6.67 mL, 8.33 mL, and 10.00 mL of STP standard solution in methanol (30 μg/mL) were successively transferred into a series of 10-mL volumetric flasks. Then, methanol was added to dilute to the volumetric flask graduation line, and Shimadzu UV-1800PC ultraviolet spectrophotometer was used to measure the absorbance of each test solution at 301 nm. The standard curve was got with the concentration (μg/mL) as the vertical axis and the absorbance value as the horizontal axis. There was a good linear relationship between concentration and absorbance in the range of 1 ~ 30 μg/mL. The standard curve equation is $C = 0.04798 + 37.08815A$ and $R^2 = 0.99982$.

In Vivo Sample Quantification

Ten microliters of 1, 5, 10, 100, 400, and 800 μg/mL STP methanol solution and 90 μL of freshly blank plasma were taken and mixed for 2 min at room temperature, respectively. After this, 100-μL internal standard (IS) xanthone solution (225 μg/mL solution) and 300 μL methanol were added into the above mixture, vortexed for 5 min, and centrifuged at 15,000 rpm for 10 min. The total mixture was filtered to get the supernatant for HPLC determination. Drug concentration in plasma was determined by Shimadzu LC-20AT series HPLC system (Kyoto, Osaka, Japan). STP was separated by a WONDASIL C18 SUPERB column (5 μm, 4.6 mm × 250 mm) at 40 °C. The injection volume was 10 μL, and the eluates were monitored at 254 nm. The mobile phase consisted of 85% methanol and 15% water pumped at a 1.0 mL/min flow rate. The standard curve was obtained with the STP absorbance ratio to the internal standard as the vertical axis and the concentration (μg/mL) as the horizontal axis. There was a good linear relationship between concentration and absorbance ratio in the range of 0.1 ~ 80 μg/mL. The standard curve equation is $A_{STP}/A_{IS} = 0.00148 + 0.00323C$ and $R^2 = 0.99959$.

Anti-acid Degradation Stability

Simulated gastric juice (*i.e.*, 0.1 N HCl without pepsin) and simulated intestinal juice (*i.e.*, pH6.8 PBS without pancreatin) were used to examine the acidolysis of free STP and STP-SDs. Aliquots of STP solution or STP-SDs (equal to 1 mg STP) were added into 10 mL SGF and SIF and kept in a shaker at 37 °C and 100 rpm. At 0, 3, 6, 12, and 24 h, 1 mL of sample solution was withdrawn, and an equal volume of fresh medium was immediately supplemented. The concentration of retained STP was analyzed by UV spectrophotometry.

Stability Test of STP-SDs

STP-SDs were placed in a penicillin bottle. The storage stability was evaluated after 3 months under room temperature (average temperature 25–28 °C) and refrigeration (4 °C), and the relative humidity was both 60–70% RH. After 3 months, the drug content of STP-SDs in water, gastric juice, and intestinal juice was measured and compared with the initial value (day 0) to evaluate its chemical stability.

In Vitro Release Study

The paddle method in the 2020 Chinese Pharmacopoeia was adopted to study the *in vitro* release of STP from SDs or effervescent tablets on the ZRS-4 intelligent dissolution tester. Briefly, the preparation equivalent to 10 mg of STP was weighed accurately and put into 500 mL newly degassed 0.1 N HCl solution and pH6.8 phosphate buffer containing 0.25% (w/v) SDS. The dissolution system was kept at 37.0 ± 0.5 °C and 100 rpm. A 6-mL sample was withdrawn and immediately replenished with a fresh medium at predetermined time points. After filtering using a 0.45-μm filter, the sample was quantified by UV spectrophotometry. The cumulative dissolved STP (%) was calculated as mean ± S.D. ($n = 3$) and plotted *versus* time.

Preparation Method Screening of Effervescent Tablets

Table I shows the formulation composition used in method screening of preparing STP-SD-ETs. The preparation methods included direct powder compression, dry granulation, and wet granulation. For the powder direct compression method, firstly, all excipients were sieved with a 100-mesh sieve and subsequently mixed with the prescribed anhydrous citric acid and mannitol for 10 min to obtain mixture 1. Similarly, the formulation amount of sodium bicarbonate was mixed with SDs for 10 min to obtain mixture 2. Finally, mixtures 1 and 2 were blended thoroughly and immediately pressed into tablets. The final solid mentioned above was crushed into coarse particles for the dry granulation method, sieved through a 20-mesh sieve for granulation, and pressed into tablets immediately according to the prescribed amount. All the ingredients were passed through a 100-mesh sieve for the wet granulation method. The formulation amount of anhydrous citric acid and mannitol was mixed for 10 min, and an appropriate amount of purified water was used as a binder to make a soft material. The soft material was passed through a 20-mesh sieve to obtain uniform wet particles, which were dried for 1 h in an oven at 60 °C, and then sieved through a 20-mesh sieve to obtain mixture 1. Simultaneously, prescribed sodium bicarbonate and the solid dispersion mix for 10 min to obtain mixture 2. Finally, the mixture 1 and 2 were thoroughly mixed and immediately pressed.

Table I The formulation composition for preparation method screening of STP-SD-ETs

Composition	Content (mg)	Function
SDs (drug/carrier = 1:5,w/w)	30	Active ingredient
Anhydrous citric acid	20	Effervescent disintegrant
Sodium bicarbonate	20	Effervescent disintegrant
Directly compressible mannitol	30	Filler & sweetener

Formulation Screening of Effervescent Tablets

Under the condition that the dosage of other ingredients remained unchanged, the influence of mannitol and lactose monohydrate alone, or the combination of both, on the powder properties and the tablet quality was studied firstly to screen the filler type. Secondly, the optimal dosage of each composition was screened by changing the SD dosage (such as 30 mg, 40 mg, 50 mg) and effervescent agent. The mass ratio of acid–base components was fixed at 1:1 and the dosage 40 mg and 30 mg, respectively. Finally, based on the optimal formulation dosage selected above, the mass ratio of acid and alkali components in effervescent agents was further investigated. The powder properties such as fluidity and compressibility were evaluated by repose angle and compressibility index. The tablet quality was mainly assessed by examining appearance, weight difference, hardness, disintegration time, etc.

Evaluation of Powder Pre-compression Performance and Tablet Quality

Angle of Repose

A fixed funnel device was applied to measure the repose angle of the powder. Briefly, the lower funnel mouth was placed 10.5 ± 0.2 cm above the plane, and a fixed volume

of powder was poured into the funnel slowly. Then, the funnel cover was opened to allow the powder to flow out, and the height (h) and bottom diameter (d) of the powder pile were recorded after all powder flowed out. The calculation formula of the repose angle (θ) is as follows:

$$\theta = \tan^{-1}(2h/d)$$

Compressibility Index and Hausner's Ratio

The compressibility index and Hausner's ratio were calculated according to the value of bulk density (δa) and tap density (δt). After the 50-g powder was put into a 100-mL measuring cup, the initial volume (V_1) was measured, and the bulk density was calculated by the formula: $\delta a = 50/V1$. The powder in the cup was shaken until it reached a fixed volume (V_2), and the formula $\delta t = 50/V2$ calculated the tap density.

$$\text{Compressibility Index}(\%) = (\delta t - \delta a)/\delta t * 100\%$$

$$\text{Hausner}'\text{s Ratio} = \delta t/\delta a$$

Disintegration Time

The disintegration time of 6 tablets was determined in 200 mL distilled water at 20 ± 5 °C, and it was considered to completely disintegrate when completely dispersed fragments were obtained, and gas release ceased. The results are average ± standard deviation. The disintegration time is considered acceptable within 5 min in 2020 Chinese Pharmacopoeia.

The pH Value of the Dispersion

The consistency of the pH value of the solution is a symbol of the uniform distribution of raw materials in the tablet. Six tablets were placed in a 50-mL beaker containing distilled water, and the temperature was maintained at 25 °C. After the tablet was completely disintegrated, the pH of the dispersion was measured.

The Moisture Contents

The 2020 Chinese Pharmacopoeia stipulates that the moisture content of tablets should be less than 0.5%. The initial weight of six effervescent tablets was weighed separately and then placed in a vacuum oven at 60 °C with a tray. The final weight was measured after drying for 48 h. The percentage of weight loss is the moisture content.

Pharmacokinetic Study

Male Sprague Dawley rats (210 ± 20 g) fasted overnight before gavage, but they could freely take water. The rats were randomly divided into the STP suspensions group and STP-SD-ETs group ($n = 5$). The STP suspensions and the suspension made from STP-SD-ETs were intragastrically administered to the rats at 40 mg/kg according to the body weight. The blood was taken from the retro-orbital venous plexus and collected into a heparinized test tube at 0.25, 0.5, 0.75, 1, 2, 4, 6, 8, 10, 12, and 24 h after administration. The blood was centrifuged at 3000 rpm for 10 min to obtain the plasma and stored at − 80 °C.

For concentration determination, the sample was deproteinized. Briefly, 100 μL freshly melted plasma was mixed with 100 μL of Xanthone solution (225 μg/mL) as an internal standard, as well as 300 μL of methanol, vortexed at room temperature for 5 min, and then centrifuged at 15,000 rpm for 10 min. After that, the supernatant was subjected to HPLC measurement. Finally, WinNonlin software (Certara USA, Inc., Princeton, NJ, USA) was used to process the data and calculate all pharmacokinetic parameters, including the maximum plasma concentration (C_{max}), the time to reach the maximum plasma concentration (T_{max}), the area under the blood concentration–time curve (AUC), and the average residence time (MRT) and relative bioavailability. The relative bioavailability calculation formula is:

$$RBA(\%) = AUCt/AUCr \cdot 100\%$$

where AUC_t and AUC_r refer to the AUC of STP-SD-ETs and STP suspensions, respectively.

In Vivo Single-Pass Intestinal Perfusion

To investigate whether the STP-SD-ETs alter (weaken or enhance) the permeability of STP to the intestine, we divided male Sprague Dawley rats (210 ± 20 g) into two groups: STP ($n = 3$) and STP-SD-ETs ($n = 3$). The rats were anesthetized by intraperitoneal injection of chloral hydrate test solution (3.3%, 1 mL/100 g), and the abdominal cavity was opened about 3 to 4 cm in length along the midline of the abdomen to expose the intestine. The duodenum segment starts at 1 cm from the pylorus and ends 10 cm downward; the jejunum segment starts at 15 cm and ends at 10 cm downwards from the pylorus; the ileum segment starts at 20 cm ascending from the cecum and ends 10 cm downwards. Two ends of each segment of the intestine were intubated and connected to the peristaltic pump. Hereafter, Krebs–Ringer buffer was utilized for draining the intestinal contents and equilibrated at a flow rate of 1 mL/min for 10 min. Subsequently, the preparation (37 °C), equivalent to 100 μg/mL

of STP prepared by diluting STP-SD-ETs or STP methanol solution into Krebs–Ringer buffer, was employed to fill the intestine, and the flow rate was reduced to 0.218 mL/min. The fluid from the outlet of each intestinal segment was collected continuously within 2 h, namely receiving fluid, while the fluid for rinsing each intestinal segment with blank Krebs–Ringer buffer after 2 h was called washing solution. Finally, the receiving fluid and the washing solution were transferred to a 100-mL volumetric flask. The rats were sacrificed, and the diameter and length of the intestinal segment were measured.

For error elimination caused by tube adsorption, STP concentration of two perfusate passing through the tube was used as the initial concentration C_0. A blank Krebs–Ringer buffer fixed the volume of the perfusion sample. Perfusion fluid (220 µL) was mixed with 780 µL methanol to dissolve STP and centrifuged at 15,000 rpm for 10 min. Afterward, 10 µL of the supernatant was injected into HPLC to determine the initial content X_0 and the remaining content X_{2h} in each intestinal segment within 2 h. The absorption rate constant (Ka) and apparent permeability coefficient (Papp) were calculated using the following formula based on the law of conservation of mass:

$$Ka = (X0 - Xt)/X0 \cdot \mathrm{Q}/(\pi r^2 l)$$

$$Papp = -Q \cdot 1n(Xt/X0)/(2\pi \mathrm{rl})$$

where Q denotes the flow rate (0.218 mL/min), r is the radius of the intestine (cm), L is the length of the perfused intestinal segment (cm), and X_0 and X_{2h} are initial drug content, and the remaining STP amount after 2 h, respectively.

RESULTS AND DISCUSSION

Preparation and Formulation Screening of STP-SDs

The impact of drug/carrier mass ratio on dissolution was examined and shown in Fig. 2. The ratio of drug to the carrier influenced the saturated solubility and dissolution of the drug in SGF and SIF. Figure 2A displayed that the higher the carrier ratio, the lower the saturated solubility of SDs in water and SGF, because the increased carrier amount strengthens the drug/polymer interaction. Nevertheless, unexpectedly, the saturated solubility in SIF showed an increasing trend and then decreased as the carrier ratio increased (Fig. 2A). By observing the phenomenon at the end of the saturation solubility determination (Fig. 2B), we analyzed that this trend may be due to the dissolved drug being hindered by the viscous gel layer formed by the Eudragit L100 dissolution and released slowly and incompletely, causing the measured saturated solubility fluctuating (30, 39). Since the carrier ratio is low initially, it might have little influence on solubility determination. As the carrier ratio increased, this hindering effect became more apparent, leading to the solubility firstly increasing and then decreasing. The 2020 Chinese Pharmacopoeia requires that the dissolution of enteric preparations in SGF should be less than 10% of the labeled amount. Additionally, it is anticipated that the cumulative dissolution of enteric formulations in SIF could be as high as possible in a short time. In summary, the optimized SD formulation (drug/carrier = 1:5, w/w) has the lowest saturated solubility in SGF, its cumulative dissolution in SGF within 2 h was less than 10% (Fig. 2C), and simultaneously, it took less time to dissolute 90% in SIF (Fig. 2D). As a result, 1:5 was selected as the final mass ratio of the drug to the carrier. The resulting STP-SDs possess an entrapment efficiency of 78% and 16% drug loading.

Solid-State Characterization of STP-SDs

SEM

The SEM examination revealed that STP crystal particles had a regular geometric shape and exhibited a rod-like structure, with a short diameter of about 15 µm and a long diameter of about 40 µm gauged from the scale bar (Fig. 3A). Since STP-SDs were prepared by rotary evaporation, they presented a thin plate-like structure with an uneven surface as revealed by SEM (Fig. 3A). Before the test, the SD was passed through an 80-mesh sieve (the pore size is 180 µm); therefore, the particle size was around 180 µm (Fig. 3A). Importantly, whether it was observed from the surface or the cross-section, the internal structure of the STP-SDs was relatively uniform, and no prominent heterogeneous components were observed, indicating the drug was uniformly dispersed in polymer to generate a uniform mixture, which effectively impeded STP from being destroyed by stomach acid.

XRD

As shown in Fig. 3B, raw STP particles had sharp crystal diffraction at 6.245°, and other minor peaks appear at 11.994°, 15.909°, 17.643°, 18.870°, 19.122°, 25.227°, and 31.697° in the 2θ range. Eudragit L100 showed weak fluctuation between 10° and 20° 2θ, but it had no crystalline peak due to its amorphous nature. The diffraction pattern of the physical mixture (PM) demonstrated the weak fluctuation of the carrier and the characteristic diffraction peaks caused by the drug, indicating that STP in PM was still in a crystalline state. Yet, the characteristic STP peak in SD disappeared and suggested that the drug was dispersed as an amorphous state. It was speculated that there might be an interaction between STP and Eudragit L100, decreasing the STP crystallinity.

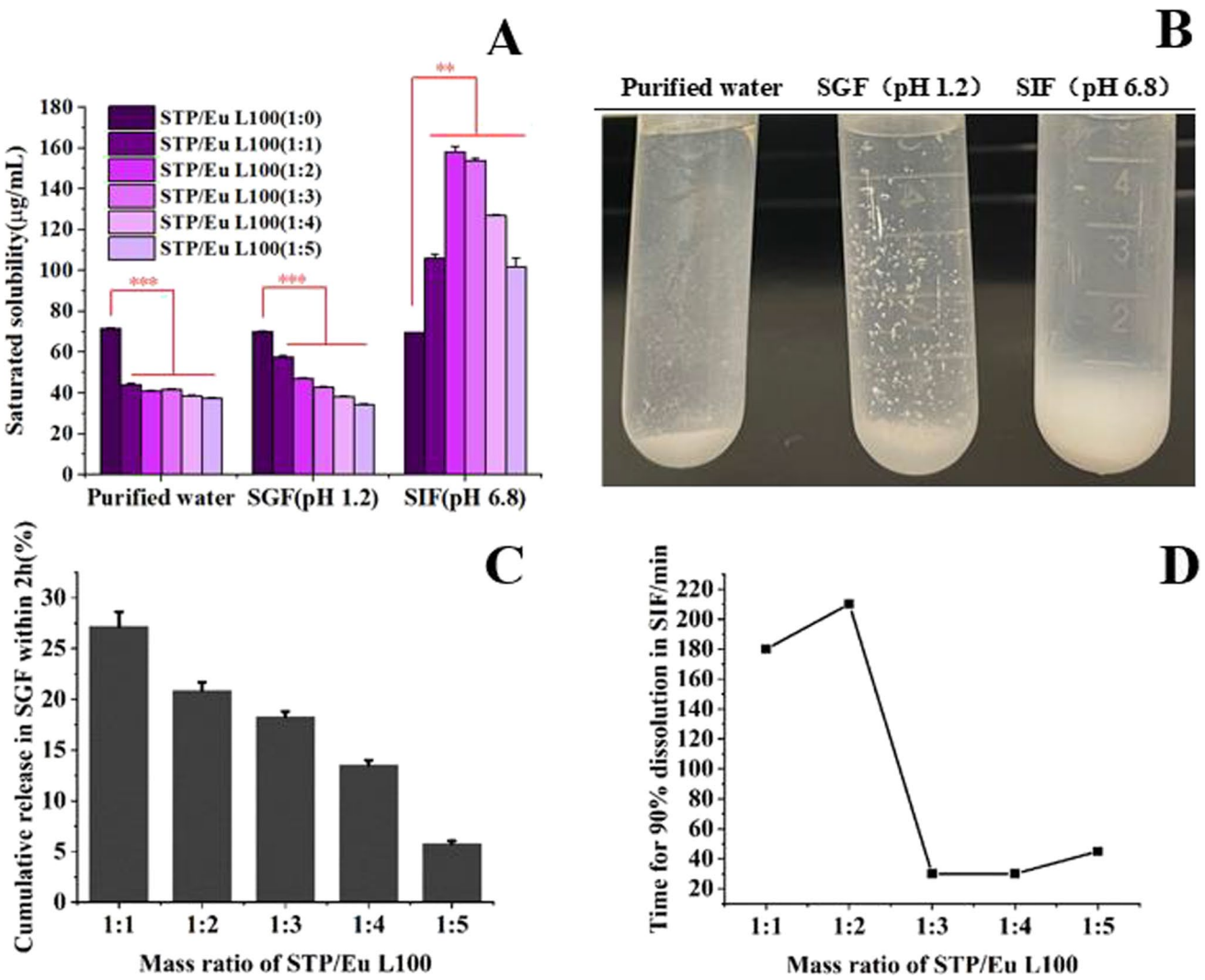

Fig. 2 Formulation screening of STP-SDs. The effect of STP/Eudragit L100 mass ratio on saturated solubility of STP-SDs ($n=3$, $^{**}P<0.01$ and $^{***}P<0.001$) (**A**), the phenomenon at the end of saturation solubility measurement (**B**), the effect of STP/Eudragit L100 mass ratio on cumulative release in SGF within 2 h ($n=3$) (**C**), and time for 90% dissolution in SIF ($n=3$) (**D**) of STP-SDs. SGF, simulated gastric fluid; SIF, simulated intestinal fluid; STP-SDs, stiripentol-loaded solid dispersions; Eu L100, Eudragit L100

DSC

DSC was performed to confirm the drug state in the SD. As shown in Fig. 3C, STP began to absorb heat at 75.1 °C and formed a sharp endothermic peak attributed to the STP melting because the melting point of STP is about 75 °C. Eudragit L100 had a broad peak near 200 °C, suggesting that the amorphous polymer changed from a glassy state to a rubbery state with enthalpy relaxation, and the temperature at which heat absorption begins was very close to the theoretical T_g (about 195 °C) of Eudragit L100. The PM curve showed all the endothermic peaks of each pure component, especially an endothermic peak corresponding to the melting point of STP, indicating that there was still crystallinity in the PM; that is, all or part of STP was still in a crystalline form. No melting peak of STP was observed in the thermal analysis chart of SD, demonstrating that during the preparation, STP changed from a crystalline state to an amorphous state and was miscible with the carrier.

FTIR

The characteristic FTIR peaks of STP are as follows(40): trisubstituted benzene ring generally exhibits C-H stretching vibration in the region of 3120–3000 cm^{-1} (i.e., 3071.2, 3035.3 cm^{-1}); the C=C stretching vibration of olefins (i.e., 1648.4, 1608.1 cm^{-1}); the C-O stretching vibration of dioxolane (i.e., 1248.3 cm^{-1}); the C=C stretching vibration of the benzene ring usually appears in the region of 1650–1430 cm^{-1} (i.e., 1648.4, 1608.1 cm^{-1}); free hydroxyl

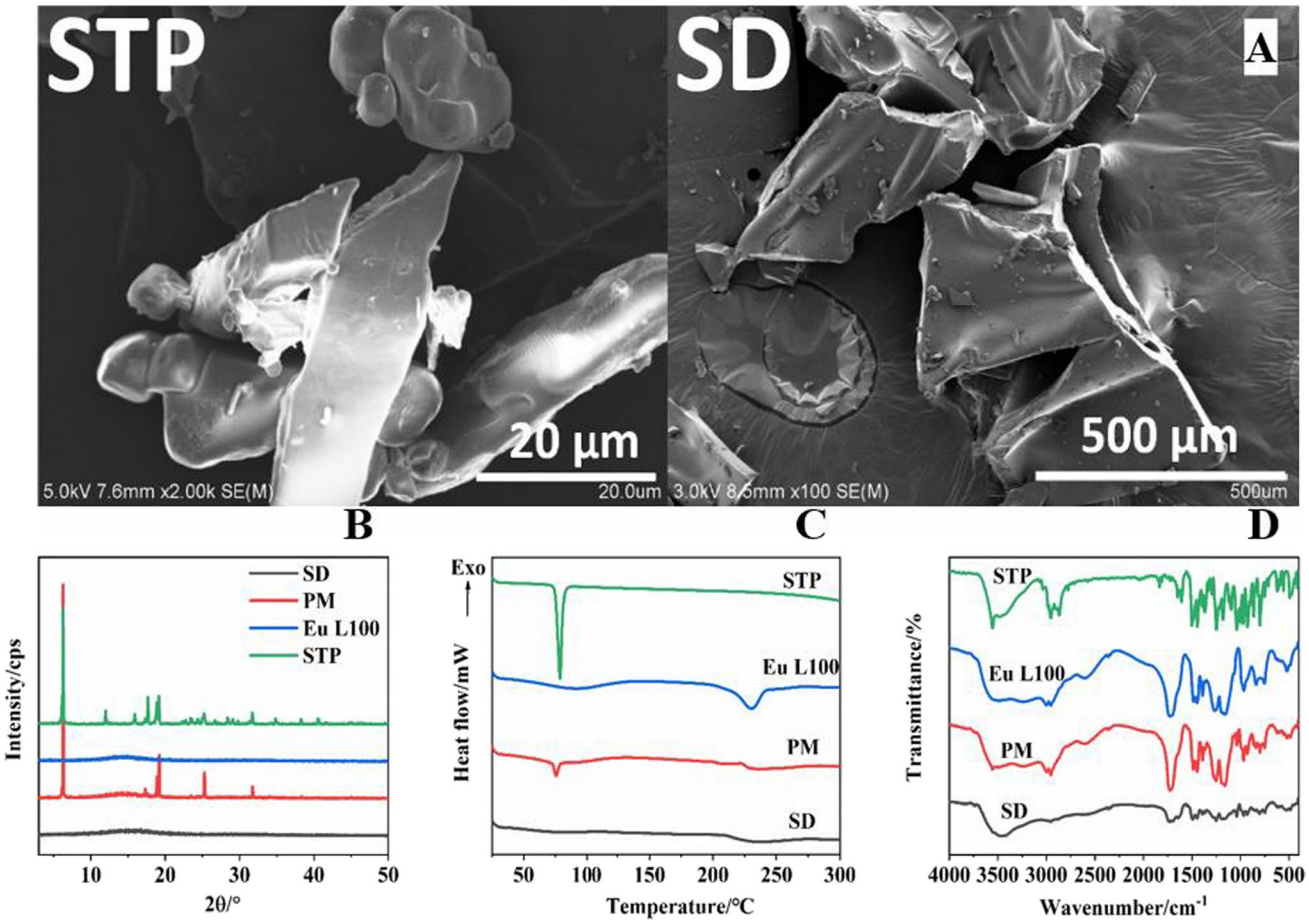

Fig. 3 Characterization of STP-SDs. **A** SEM, **B** PXRD, **C** DSC, and **D** FTIR. STP-SDs, stiripentol-loaded solid dispersions; PM, physical mixture; Eu L100, Eudragit L100; SEM, scanning electron microscopy; PXRD, powder X-ray diffraction; DSC, differential scanning calorimetry; FTIR, Fourier-transform infrared spectroscopy

has strong absorption in the region of 3600–3500 cm^{-1} (i.e., 3553.9, 3482.1 cm^{-1}), but intra- or intermolecular hydrogen bonds will reduce the stretching wave number of O–H to the region of 3550–3200 cm^{-1}. The characteristic peaks of Eudragit L100 are primarily the stretching vibration of the free hydroxyl group (3487.8, 3237.7 cm^{-1}), the stretching vibration of C = O (1726.5 cm^{-1}), the stretching vibration of C-O of the carboxyl group (1266.5 cm^{-1}), the asymmetric stretching vibration (1266.5 cm^{-1}) and the symmetric stretching vibration of C–O–C (1160.7 cm^{-1}). In the PM infrared spectrum, the characteristic area (4000 ~ 1250 cm^{-1}) and the fingerprint area (1250 ~ 400 cm^{-1}) were superpositions of the STP and Eudragit L100 spectra, suggesting there was no interaction between them. Compared with raw STP crystals, the oxygen-hydrogen single bond stretching vibration peak (3600 ~ 3200 cm^{-1}) and the carbon-hydrogen double bond stretching vibration peak (~ 1728 cm^{-1}) in SD showed a wider absorption band, mainly due to the formation of hydrogen bonds between the secondary hydroxyl group or benzoxazole moiety of STP and the carboxyl or carbonyl groups of the polymeric carrier (40). Additionally, hydrogen bond association often causes the carbon-hydrogen single bond stretching vibration peak (3000 ~ 2850 cm^{-1}) to be submerged and only the top of the peak being exposed, proving that the two are evenly dispersed in the carrier through the hydrogen bond interaction. This favorable intermolecular interaction might drive STP to maintain an amorphous state for a long time, thereby hindering the crystallization behavior during storage (41).

Anti-acid Stability of STP-SDs

After 24-h exposure to the gastric environment, the STP absorbance at 301 nm decreased (Fig. 4A). In contrast, the absorbance in intestinal fluid had no alteration (Fig. 4B), demonstrating that under different conditions (degraded and undegraded), the change in absorbance intensity of STP can be used to evaluate its stability. As shown in Fig. 4C, after 6-h incubation in gastric juice, the remaining drug in the

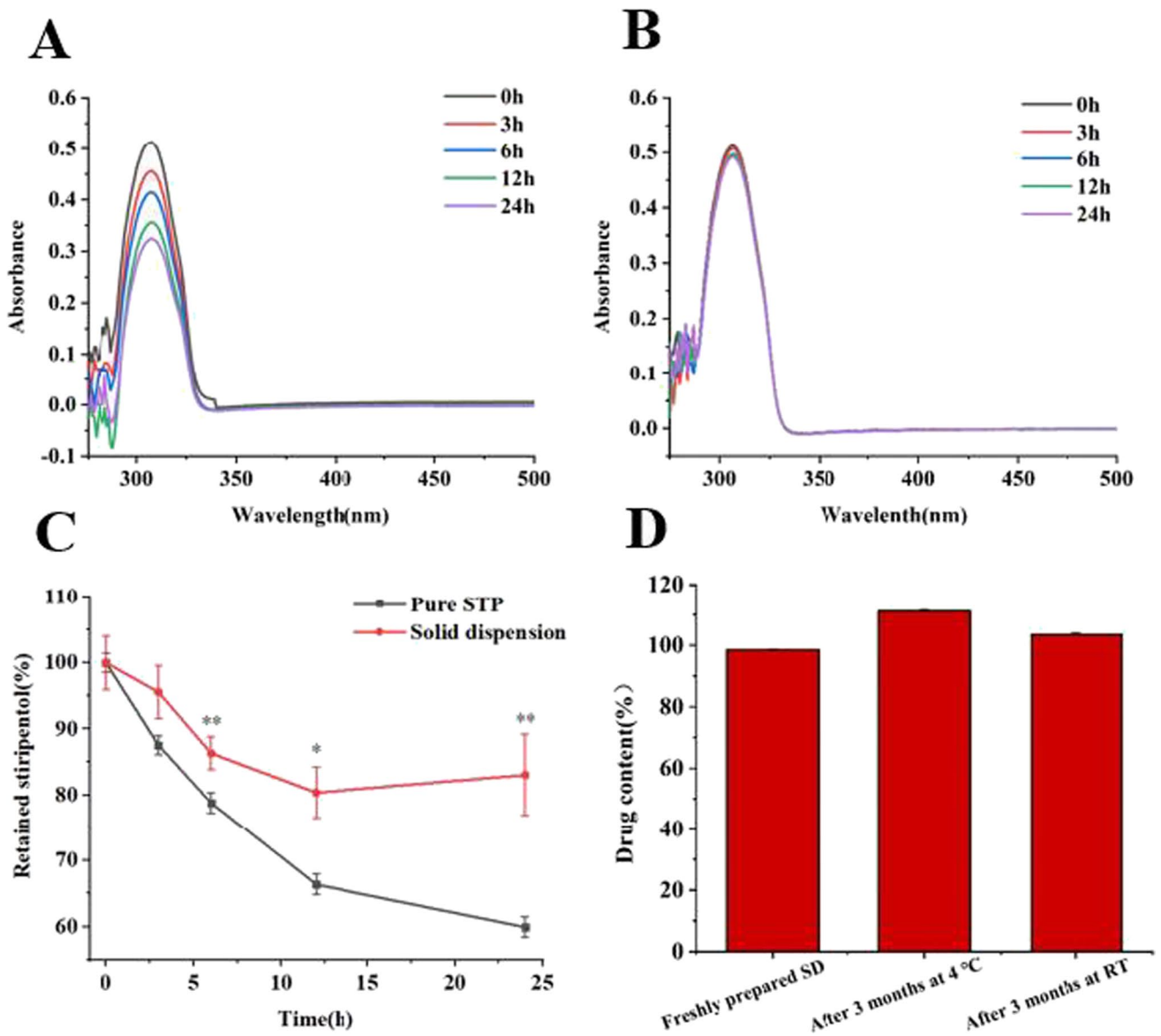

Fig. 4 Stability of free STP in SGF and SIF (**A** and **B**), acidic destabilization curves of free STP and STP-SDs in SGF (*$P<0.05$ and **$P<0.01$) (**C**), the chemical stability of STP-SDs characterized by drug content for 3 months (**D**). $n=3$, mean ± S.D. STP-SDs, stiripentol-loaded solid dispersions; SGF, simulated gastric fluid; SIF, simulated intestinal fluid; RT, room temperature

STP-SDs group was higher than that in the free drug group, while only 59.92% STP in the free-drug group remained after 24 h. However, the STP amount in enteric SDs decreased slightly within 12 h, then reached an unchanged level, and the drug retention percentage was 83.06% after 24-h exposure. The degradation in the first 12-h period may be due to the free drug on the SD surface. At 2 h after incubation in SGF, only 91.69% STP stayed in the pure STP group, while the SD had 97.02% STP remaining. Moreover, the drug content in STP-SDs after 3-month storage under various storage conditions has no significant difference compared to the initial value (Fig. 4D, independent sample *t*-test, $P>0.05$). The results demonstrated that the enteric SDs could effectively improve the STP anti-acid hydrolysis ability and chemical stability.

Preparation Method Screening of Effervescent Tablet

The effervescent tablets prepared by the three methods, direct powder compression, dry granulation and tableting, and wet granulation and tableting, demonstrated a similar appearance (Figure S1). All of them were intact, smooth, and uniform in color without sticking or cracking (Figure S1). As displayed in Table S1, the weight difference of various tablets all conformed to the requirements of the

2020 Chinese Pharmacopoeia, illustrating that the powder possesses superior fluidity and compressibility. The hardness of the tablets was within the range of 50–85 N, thereby ensuring the integrity of the preparation during storage and usage. The disintegration time of all was far less than 5 min stipulated in the 2020 Chinese Pharmacopoeia, and the effervescent tablet prepared by dry granulation disintegrated fastest with the greatest hardness. Therefore, dry granulation was selected as the preparation method.

Formulation Screening of Effervescent Tablet

When the angle of repose is 25–30°, the compressibility index is in the range of 5–16%, as well as Hausner's ratio is lower than 1.18, it indicates that the powder holds superior fluidity. The filler type was screened by studying the influence of a single filler or a combination on the powder fluidity and compressibility. Based on the formulation composition present in Table II, the fluidity and compressibility of the powder obtained by utilizing direct pressure mannitol was better than lactose monohydrate or a mixture of them (Fig. 5A and B), by comparing F3 with F4 and F5, F6 with F7, F8 with F9, and F10 with F11. This can be explained by the fact that mannitol is prepared by spray drying, allowing a loose and porous structure for compression. Next, we optimized the formulation by changing the SD dosage (such as 30 mg, 40 mg, and 50 mg) and effervescent dosage (the mass ratio of acid–base components was fixed at 1:1, and the dosage was 40 mg or 30 mg) by comparison among formulations

Table II The formulation composition for screening filler types, the dosage of each ingredient, and effervescent acid–base ratio of STP-SD-ETs

Formulation	SDs (drug/carrier = 1:5, w/w)/(mg)	Anhydrous citric acid/(mg)	Sodium bicarbonate/(mg)	Directly compressible mannitol/(mg)	Lactose monohydrate/(mg)
F1	30	13.33	26.67	30	-
F2	30	26.67	13.33	30	-
F3	30	20	20	30	-
F4	30	20	20	-	30
F5	30	20	20	15	15
F6	40	15	15	30	-
F7	40	15	15	-	30
F8	40	20	20	20	-
F9	40	20	20	-	20
F10	50	15	15	20	-
F11	50	15	15	-	20

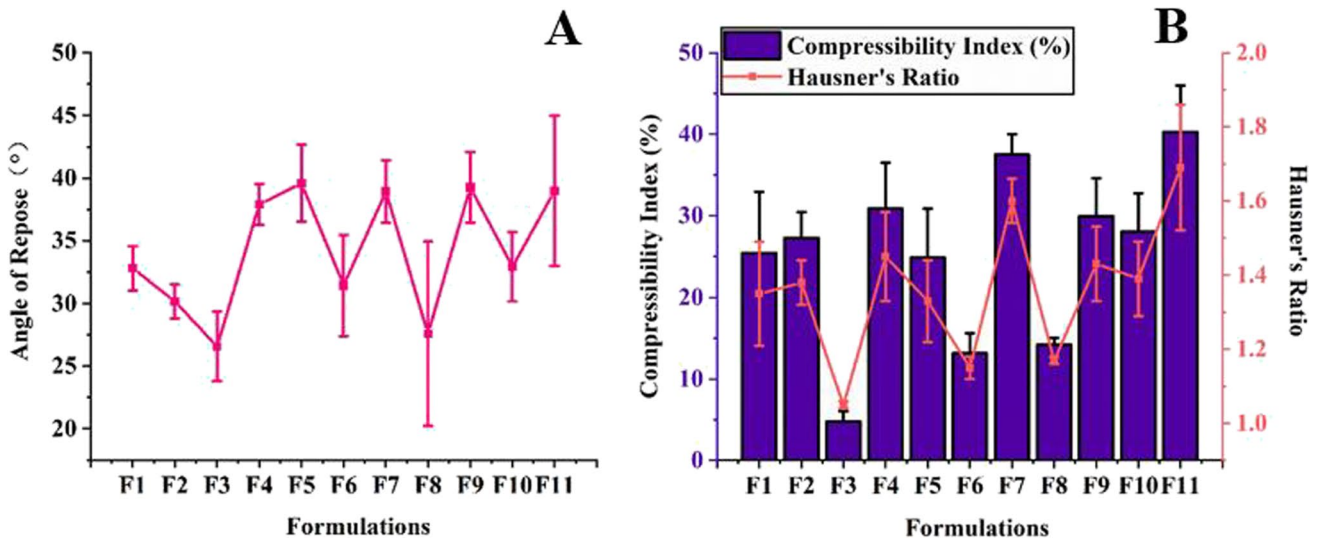

Fig. 5 Evaluation of powder performance during formulation screening. **A** Angle of repose, **B** compressibility index, and Hausner's ratio; F1, the formulation one

F3, F6, F8, and F10. The formulation with SD/effervescent agent/filler ratio of 30:40:30 (w/w/w) exhibited the best performance in terms of fluidity and compressibility. Based on the optimal formulation dosage selected above, the mass ratio of acid–base components was further investigated. The powder evaluation of F1, F2, and F3 showed that the 1:1 mass ratio of acid–base components displayed improved powder performance. Most importantly, F3 demonstrated the highest hardness and the shortest disintegration time (Fig. S2B and C), whereas there was no significant difference in tablet weight and pH of dispersion among all formulations (Fig. S2A and D). Taken together, F3 was selected as the optimal formulation for the subsequent study.

Quality Examination of the Optimal Tablet and Dissolution Behavior

Quality examination of the optimized tablet was shown in Table S2. All the determination parameters met the requirements in the 2020 Chinese Pharmacopoeia. As depicted in Fig. 6, the optimal STP-SD-ETs and STP-SDs displayed similar dissolution behavior and indicated that pressing STP-SDs into an effervescent tablet did not affect dissolution performance. STP suspensions only released about 70% at 5.5 h in SIF and showed 60% dissolution in SGF at 0.5 h, whereas STP-SD-ETs and STP-SDs allowed 90% accumulative dissolution within 0.5 h in SIF and less than 10% dissolution in SGF at 2 h. The results indicated that STP-SD-ETs improved the STP dissolution and its stability in gastric fluid.

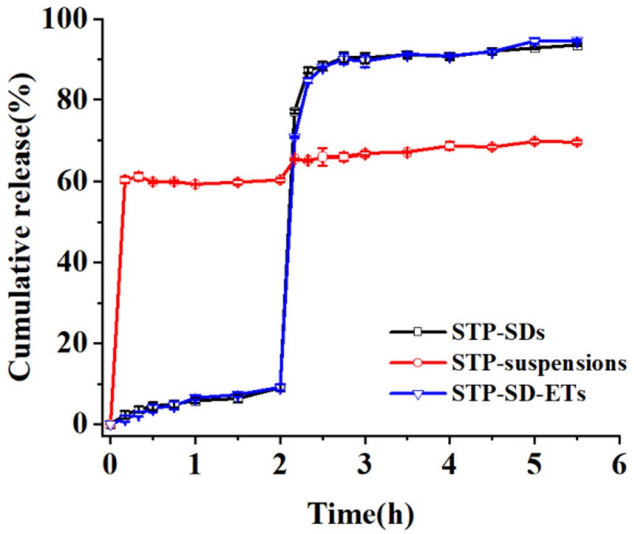

Fig. 6 The dissolution profiles of STP from STP suspensions, solid dispersions, and effervescent tablets were performed in 0.1 N HCl (the first 2 h) and pH 6.8 phosphate buffer (from 2 to 5.5 h) ($n=3$). STP-SD-ETs, effervescent tablets containing enteric stiripentol-loaded solid dispersions

Pharmacokinetic Study

The plasma concentration of STP *vs*. time curve was shown in Fig. 7, and the pharmacokinetic parameters were summarized in Table III. The plasma concentration of the STP suspension group reached the C_{max} at 0.25 h and declined rapidly after administration. In contrast, STP-SD-ETs reached maximal plasma concentration at around 1.55 h due to the delayed-release characteristics of enteric material. Meanwhile, STP-SD-ETs demonstrated higher AUC (29.99 μg·h/mL) than STP suspensions (21.62 μg·h/mL). The results showed that formulating STP into SD-ETs endowed the drug with delayed-release properties, thus significantly improving the bioavailability.

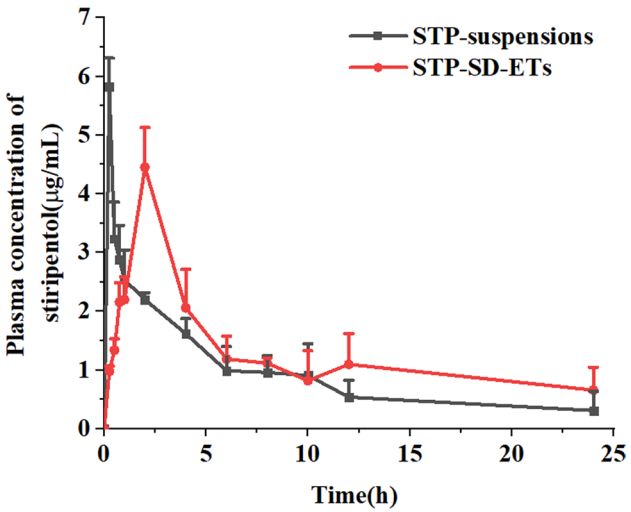

Fig. 7 The STP plasma concentration *versus* time profiles in rats following oral administration (at a dose of 40 mg/kg) of STP suspensions and STP-SD-ETs ($n=5$). STP-SD-ETs (Enteric), effervescent tablets containing enteric stiripentol-loaded solid dispersions

Table III Main pharmacokinetic parameters of STP in Sprague Dawley rats after oral administration (at a dose of 40 mg/kg) of STP suspensions and STP-SD-ETs. $n=5$, $^{**}P<0.01$ and $^{\#\#}P<0.01$

Formulations	STP suspensions	STP-SD-ETs
C_{max} (μg/mL)	5.83 ± 0.48	3.65 ± 1.21
T_{max} (hour)	0.25 ± 0.00	1.55 ± 0.62**
$AUC_{0\text{-}t}$ (μg·h/mL)	21.62 ± 4.32	29.99 ± 3.35##
RBA (%)	N/A	138.71

C_{max}, maximum concentration; *T_{max}*, peak time; *AUC*, area under the plasma STP concentration–time curve; *RBA*, relative bioavailability calculated based on AUC_{0-t}; *STP-SD-ETs*, effervescent tablets containing enteric stiripentol-loaded solid dispersions.

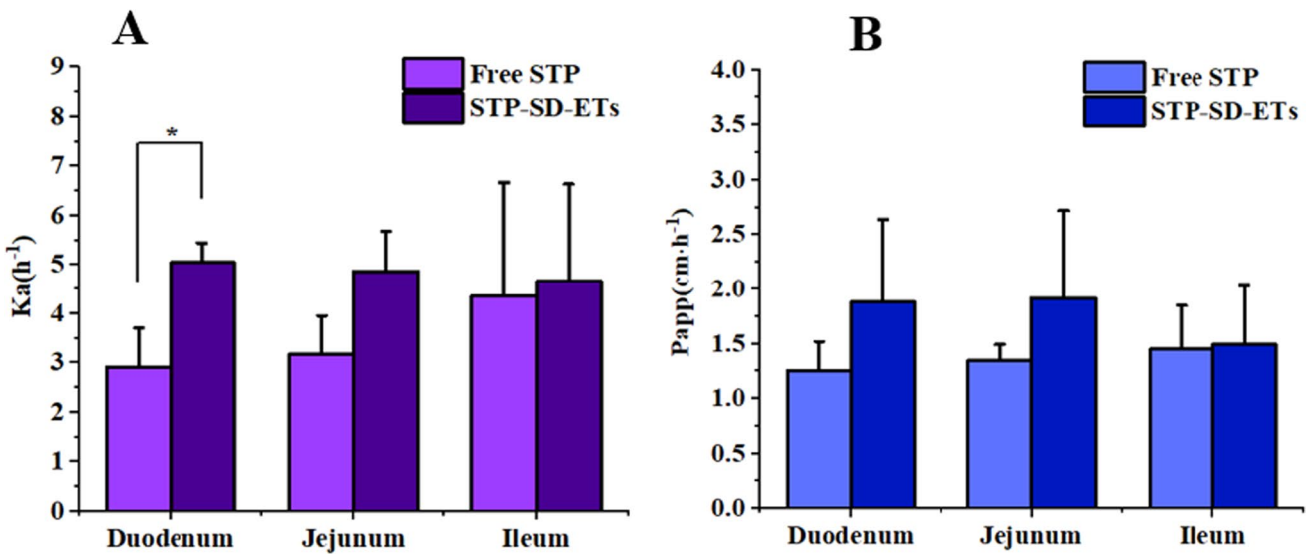

Fig. 8 The absorption rate constant (Ka) and the apparent permeability coefficient (Papp) of STP and STP-SD-ETs were evaluated by the *in vivo* single-pass intestinal perfusion ($n=3$). One-way ANOVA, *significantly different from free STP ($^*P<0.05$). STP-SD-ETs, effervescent tablets containing enteric STP-loaded solid dispersions

Intestinal Permeability

Permeability is a critical indicator for studying the drug penetration through the intestine, reflecting the ability of the active drug ingredients to be absorbed (30). The absorption rate constant (Ka) and the apparent permeability coefficient (Papp) of free STP and STP-SD-ETs (enteric) were given in Fig. 8A and B. STP is a BCS II drug and exhibited good permeability in different intestinal segments. So, there was no significant difference in Papp (Fig. 8B). The data in Fig. 8A indicated that the absorption rate of free drug varied in different intestinal segments, while STP in STP-SD-ETs was well absorbed in all intestinal segments. Besides, the Ka of STP-SD-ETs in the duodenum was significantly higher than that of free STP. This improvement in absorption rate may be attributed to the "water-resistant" interaction between drug and polymer, which can effectively inhibit drug crystallization in aqueous solution and keep the drug supersaturation (42). Moreover, the supersaturation maintenance resulting from STP-SD-ETs can be converted into an enhanced flux of drug molecules across the membrane (43, 44). The results indicated that STP-SD-ETs allowed enhancement in membrane permeability and intestinal absorption.

CONCLUSIONS

This study has developed an innovative oral formulation of STP based on enteric solid dispersions and effervescent tablets. The formulation has advantages including but not limited to readily available and recognized safe materials used, as well as relatively high drug loading (16%). The saturated solubility of the optimal SD formulation (STP/Eu 100 = 1:5, w/w) is about twice as high relative to the pure STP. This could be attributed to the hydrogen bond between STP and Eudragit L100, which made STP uniformly distributed in the enteric carrier and maintain its amorphous state. The optimal STP-SDs displayed less than 10% drug release in simulated gastric juice within 2 h, while about 90% dissolution within 0.5 h in simulated intestinal juice, meeting the requirements of the 2020 Chinese Pharmacopoeia for delayed-release preparations. The dissolution behavior and anti-acid degradation test illustrated that STP-SDs manifest superior protection against acid instability and have acceptable chemical stability. The STP-SD-ETs demonstrated higher bioavailability and absorption rate constant (Ka) than STP suspension formulation. In short, the oral preparations encompassing enteric solid dispersion combined with effervescent tablet technology possessed excellent performance in enhancing dissolution, anti-acid hydrolysis stability, and absorption of STP, which is expected to become a promising method to solve the problems related to the stability, solubility, and permeability reduction.

Supplementary Information The online version contains supplementary material available at https://doi.org/10.1208/s12249-022-02261-5.

Author Contributions Wei He and Jun Li conceived and designed the research work. Ying Wing, Siyuan Xu, Ziyue Xiao, Yuxin Jiang, and Qi Jiang performed the experiment. Wei He and Ying Wang co-wrote the paper. All of the authors discussed the results and commented on

the manuscript. All of the authors have read and approved the final manuscript.

Funding This study was supported by the National Natural Science Foundation of China (Nos. 81872823, and 82073782), the Shanghai Science and Technology Committee (No. 19430741500), and the Key Laboratory of Modern Chinese Medicine Preparation of Ministry of Education of Jiangxi University of Traditional Chinese Medicine (zdsys-202103).

Declarations

Conflict of Interest The authors declare no competing interests.

References

1. Trabs N, Trabs M, Stodieck S, House PM. Influence of stiripentol on perampanel serum levels. Epilepsy Res. 2020;164:106367. https://doi.org/10.1016/j.eplepsyres.2020.106367.
2. Chiron C. Stiripentol for the treatment of seizures associated with Dravet syndrome. Expert Rev Neurother. 2019;19(4):301–10. https://doi.org/10.1080/14737175.2019.1593142.
3. Eschbach K, Knupp KG. Stiripentol for the treatment of seizures in Dravet syndrome. Expert Rev Clin Pharmacol. 2019;12(5):379–88. https://doi.org/10.1080/17512433.2019.1605904.
4. Selvarajah A, Zulfiqar-Ali Q, Marques P, Rong M, Andrade DM. A systematic review of adults with Dravet syndrome. Seizure. 2021;87:39–45. https://doi.org/10.1016/j.seizure.2021.02.025.
5. Wheless JW, Fulton SP, Mudigoudar BD. Dravet Syndrome: a review of current management. Pediatr Neurol. 2020;107:28–40. https://doi.org/10.1016/j.pediatrneurol.2020.01.005.
6. Buck ML, Goodkin HP. Stiripentol: a novel antiseizure medication for the management of Dravet syndrome. Ann Pharmacother. 2019;53(11):1136–44. https://doi.org/10.1177/1060028019856008.
7. Frampton JE. Stiripentol: a review in Dravet syndrome. Drugs. 2019;79(16):1785–96. https://doi.org/10.1007/s40265-019-01204-y.
8. Nabbout R, Chemaly N, Chiron C, Kuchenbuch M. Safety considerations selecting antiseizure medications for the treatment of individuals with Dravet syndrome. Expert Opin Drug Saf. 2021;20(5):561–76. https://doi.org/10.1080/14740338.2021.1890025.
9. Gilmartin CGS, Dowd Z, Parker APJ, Harijan P. Interaction of cannabidiol with other antiseizure medications: a narrative review. Seizure. 2021;86:189–96. https://doi.org/10.1016/j.seizure.2020.09.010.
10. Stiripentol:Uses,Interactions,Mechanism of Action. https://go.drugbank.com/drugs/DB09118. Accessed 2021.
11. Johannessen Landmark C, Potschka H, Auvin S, Wilmshurst JM, Johannessen SI, Kasteleijn-NolstTrenité D, *et al*https://doi.org/10.1111/epi.16849.
12. Wang X, Mohammad IS, Fan L, Zhao Z, Nurunnabi M, Sallam MA, *et al*. Delivery strategies of amphotericin B for invasive fungal infections. Acta Pharm Sin B. 2021;11(8):2585–604. https://doi.org/10.1016/j.apsb.2021.04.010.
13. He W, Kapate N, Shields CW, Mitragotri S. Drug delivery to macrophages: a review of targeting drugs and drug carriers to macrophages for inflammatory diseases. Adv Drug Deliv Rev. 2020;165–166:15–40. https://doi.org/10.1016/j.addr.2019.12.001.
14. Zhang X, Wang H, Zhang T, Zhou X, Wu B. Exploring the potential of self-assembled mixed micelles in enhancing the stability and oral bioavailability of an acid-labile drug. Eur J Pharm Sci. 2014;62:301–8. https://doi.org/10.1016/j.ejps.2014.06.008.
15. Tai Z, Huang Y, Zhu Q, Wu W, Yi T, Chen Z, *et al*. Utility of pickering emulsions in improved oral drug delivery. Drug Discov Today. 2020;25(11):2038–45. https://doi.org/10.1016/j.drudis.2020.09.012.
16. Xiao Q, Zhu X, Yuan Y, Yin L, He W. A drug-delivering-drug strategy for combined treatment of metastatic breast cancer. Nanomed Nanotechnol Biol Med. 2018;14(8):2678–88. https://doi.org/10.1016/j.nano.2018.06.012.
17. Thapa Magar K, Boafo GF, Li X, Chen Z, He W. Liposome-based delivery of biological drugs. Chin Chem Lett. 2021. https://doi.org/10.1016/j.cclet.2021.08.020.
18. Dai Q, Zhang P, Jin Y, Tang M, Shen M, Xu S, *et al*. Using self-nanoemulsifying system to improve oral bioavailability of a pediatric antiepileptic agent stiripentol: formulation and pharmacokinetics studies. AAPS PharmSciTech. 2020;21(5):192. https://doi.org/10.1208/s12249-020-01730-z.
19. Lu R, Liu S, Wang Q, Li X. Nanoemulsions as novel oral carriers of stiripentol: insights into the protective effect and absorption enhancement. Int J Nanomed. 2015;10:4937–46. https://doi.org/10.2147/IJN.S87471.
20. He W, Wang Y, Lv Y, Xiao Q, Ye L, Cai B, *et al*. Denatured protein stabilized drug nanoparticles: tunable drug state and penetration across the intestinal barrier. J Mater Chem B. 2017;5(5):1081–97. https://doi.org/10.1039/C6TB02577C.
21. Tekade AR, Yadav JN. A review on solid dispersion and carriers used therein for solubility enhancement of poorly water soluble drugs. Adv Pharm Bull. 2020;10(3):359–69. https://doi.org/10.34172/apb.2020.044.
22. Fang R, Liu Y, Ma L, Yu X, Jin Y. Facile preparation of solid dispersions by dissolving drugs in N-vinyl-2-pyrrolidone and photopolymerization. Mater Sci Eng C. 2021;124:112063. https://doi.org/10.1016/j.msec.2021.112063.
23. Mustapha O, Kim KS, Shafique S, Kim DS, Jin SG, Seo YG, *et al*. Comparison of three different types of cilostazol-loaded solid dispersion: physicochemical characterization and pharmacokinetics in rats. Colloids Surf B. 2017;154:89–95. https://doi.org/10.1016/j.colsurfb.2017.03.017.
24. Song B, Wang J, Lu S-J, Shan L-N. Andrographolide solid dispersions formulated by Soluplus to enhance interface wetting, dissolution, and absorption. J Appl Polym Sci. 2020;137(6):48354. https://doi.org/10.1002/app.48354.
25. Zhai X, Li C, Lenon GB, Xue CCL, Li W. Preparation and characterisation of solid dispersions of tanshinone IIA, cryptotanshinone and total tanshinones. Asian J Pharm Sci. 2017;12(1):85–97. https://doi.org/10.1016/j.ajps.2016.08.004.
26. Simonazzi A, Cid AG, Paredes AJ, Schofs L, Gonzo EE, Palma SD, *et al*. Development and in vitro evaluation of solid dispersions as strategy to improve albendazole biopharmaceutical behavior. Ther Deliv. 2018;9(9):623–38. https://doi.org/10.4155/tde-2018-0037.
27. Tran PHL, Tran TTD. Dosage form designs for the controlled drug release of solid dispersions. Int J Pharm. 2020;581:119274. https://doi.org/10.1016/j.ijpharm.2020.119274.
28. Fan W, Zhang X, Zhu W, Di L. The preparation of curcumin sustained-release solid dispersion by hot-melt extrusion—II. Optimization of Preparation Process and Evaluation In Vitro and In Vivo. J Pharm Sci. 2020;109(3):1253–60. https://doi.org/10.1016/j.xphs.2019.11.020.
29. Lee H-J, Kim J-Y, Park S-H, Rhee Y-S, Park C-W, Park E-S. Controlled-release oral dosage forms containing nimodipine solid dispersion and hydrophilic carriers. J Drug Deliv Sci Technol. 2017;37:28–37. https://doi.org/10.1016/j.jddst.2016.11.001.
30. Agafonov M, Ivanov S, Terekhova I. Improvement of pharmacologically relevant properties of methotrexate by solid dispersion

with Pluronic F127. Mater Sci Eng C. 2021;124:112059. https://doi.org/10.1016/j.msec.2021.112059.
31. Sim T, Lim C, Lee JW, Kim DW, Kim Y, Kim M, *et al*. Characterization and pharmacokinetic study of itraconazole solid dispersions prepared by solvent-controlled precipitation and spray-dry methods. J Pharm Pharmacol. 2017;69(12):1707–15. https://doi.org/10.1111/jphp.12805.
32. Liang Q, Wang YR, Deng YY. Effect of HPMCAS/curcumin amorphous solid dispersion in enhancing dissolution and chemical stability of curcumin. Zhongguo Zhong Yao Za Zhi. 2019;44(15):3305–11. https://doi.org/10.19540/j.cnki.cjcmm.20190516.301.
33. Huang Y, Dai W-G. Fundamental aspects of solid dispersion technology for poorly soluble drugs. Acta Pharm Sin B. 2014;4(1):18–25. https://doi.org/10.1016/j.apsb.2013.11.001.
34. Stegemann S, Leveiller F, Franchi D, de Jong H, Lindén H. When poor solubility becomes an issue: from early stage to proof of concept. Eur J Pharm Sci. 2007;31(5):249–61. https://doi.org/10.1016/j.ejps.2007.05.110.
35. Zhang J, Han R, Chen W, Zhang W, Li Y, Ji Y, *et al*. Analysis of the literature and patents on solid dispersions from 1980 to 2015. Molecules. 2018;23(7):1697.
36. Zhao F, Li M, Meng L, Yu J, Zhang T. Characteristics of effervescent tablets of Lactobacilli supplemented with Chinese Ginseng (Panax ginseng CA Meyer) and Polygonatum sibiricum. Appl Sci (Basel). 2020;10(9). https://doi.org/10.3390/app10093194.
37. Aslani A, Sharifian T. Formulation, characterization and physicochemical evaluation of amoxicillin effervescent tablets. Adv Biomed Res. 2014;3(1):209. https://doi.org/10.4103/2277-9175.143252.
38. Aslani A, Jahangiri H. Formulation, characterization and physicochemical evaluation of ranitidine effervescent tablets. Adv Pharm Bull. 2013;3(2):315–22. https://doi.org/10.5681/apb.2013.051.
39. Xu H, Liu L, Li X, Ma J, Liu R, Wang S. Extended tacrolimus release via the combination of lipid-based solid dispersion and HPMC hydrogel matrix tablets. Asian J Pharm Sci. 2019;14(4):445–54. https://doi.org/10.1016/j.ajps.2018.08.001.
40. Almutairi MS, Leenaraj DR, Ghabbour HA, Joe IH, Attia MI. Spectroscopic identification, structural features, Hirshfeld surface analysis and molecular docking studies on stiripentol: An orphan antiepileptic drug. J Mol Struct. 2019;1180:110–8. https://doi.org/10.1016/j.molstruc.2018.11.088.
41. Paudel A, Worku ZA, Meeus J, Guns S, Van den Mooter G. Manufacturing of solid dispersions of poorly water soluble drugs by spray drying: formulation and process considerations. Int J Pharm. 2013;453(1):253–84. https://doi.org/10.1016/j.ijpharm.2012.07.015.
42. Shi Q, Li F, Yeh S, Moinuddin SM, Xin JB, Xu J, *et al*. Recent advances in enhancement of dissolution and supersaturation of poorly water-soluble drug in amorphous pharmaceutical solids: a review. AAPS PharmSciTech. 2021;23(1):19. https://doi.org/10.1208/s12249-021-02137-0.
43. Dahan A, Beig A, Lindley D, Miller JM. The solubility-permeability interplay and oral drug formulation design: two heads are better than one. Adv Drug Deliv Rev. 2016;101:99–107. https://doi.org/10.1016/j.addr.2016.04.018.
44. Beig A, Miller JM, Lindley D, Carr RA, Zocharski P, Agbaria R, *et al*. head-to-head comparison of different solubility-enabling formulations of etoposide and their consequent solubility-permeability interplay. J Pharm Sci. 2015;104(9):2941–7. https://doi.org/10.1002/jps.24496.
45. Wang X, Dong Y, Song R, Yu A, Wei J, Fan Q, *et al*. Intestinal metabolism and absorption mechanism of multi-components in Gaultheria leucocarpa var. yunnanensis - An assessment using in situ and in vitro models, comparing gut segments in pathological with physiological conditions. J Ethnopharmacol. 2022;286:114844. https://doi.org/10.1016/j.jep.2021.114844.
46. Liu YY, Zhang SD, Xiao JJ, Feng WZ, Wei D, Deng YJ, *et al*. Gut microbiota-involved metabolism and intestinal absorption mechanisms in decreasing bioaccessibility of triadimefon in strawberry and grape. Food Chem. 2022;373:8. https://doi.org/10.1016/j.foodchem.2021.131575.
47. Gao Y, He L, Katsumi H, Sakane T, Fujita T, Yamamoto A. Improvement of intestinal absorption of insulin and water-soluble macromolecular compounds by chitosan oligomers in rats. Int J Pharm. 2008;359(1):70–8. https://doi.org/10.1016/j.ijpharm.2008.03.016.